LETTER

doi:10.1038/nature10196

Attosecond control of electrons emitted from a nanoscale metal tip

Michael Krüger[1]*, Markus Schenk[1]* & Peter Hommelhoff[1]

Attosecond science is based on steering electrons with the electric field of well controlled femtosecond laser pulses[1]. It has led to the generation of extreme-ultraviolet pulses[2] with a duration of less than 100 attoseconds (ref. 3; 1 as = 10^{-18} s), to the measurement of intramolecular dynamics (by diffraction of an electron taken from the molecule under scrutiny[4,5]) and to ultrafast electron holography[6]. All these effects have been observed with atoms or molecules in the gas phase. Electrons liberated from solids by few-cycle laser pulses are also predicted[7,8] to show a strong light-phase sensitivity, but only very small effects have been observed[14]. Here we report that the spectra of electrons undergoing photoemission from a nanometre-scale tungsten tip show a dependence on the carrier-envelope phase of the laser, with a current modulation of up to 100 per cent. Depending on the carrier-envelope phase, electrons are emitted either from a single sub-500-attosecond interval of the 6-femtosecond laser pulse, or from two such intervals; the latter case leads to spectral interference. We also show that coherent elastic re-scattering of liberated electrons takes place at the metal surface. Owing to field enhancement at the tip, a simple laser oscillator reaches the peak electric field strengths required for attosecond experiments at 100-megahertz repetition rates, rendering complex amplified laser systems dispensable. Practically, this work represents a simple, extremely sensitive carrier-envelope phase sensor, which could be shrunk in volume to about one cubic centimetre. Our results indicate that the attosecond techniques developed with (and for) atoms and molecules can also be used with solids. In particular, we foresee subfemtosecond, subnanometre probing of collective electron dynamics (such as plasmon polaritons[9]) in solid-state systems ranging in scale from mesoscopic solids to clusters and to single protruding atoms.

A nanoscale solid-state system is also of interest for applications. Steering electrons with the force exerted by a synthesized few-cycle light field is predicted to allow ultimate speeds to be reached in electronics: that is, up to optical frequencies, with a typical timescale of femtoseconds ('lightwave electronics'[10], so called by analogy to microwave electronics with semiconductor chips). However, typical electron energies in conventional electronics lie in the range of a few electron volts, corresponding to a free-electron velocity of $\sim$1 nm fs^{-1}. Thus, the possible speed-up to optical frequencies in electronics can only be achieved if a nanometre-scale solid-state system is used[8]. Because the electron current is switched on and off by the light field, such a device could be called an optical attosecond field-effect transistor. The present work is, to our knowledge, the first research along these lines.

Our experiment centres on a metal tip of radius $\sim$10–20 nm, the apex of which lies in the focus of a linearly polarized laser beam that consists of few-cycle laser pulses (Fig. 1). The tip is beneficial for two reasons. First, electric field enhancement takes place because of its sharpness [11]. At the tip's apex, the electric field is around five times higher than in the laser focus alone; this corresponds to a $\sim$25-fold increase in intensity. A laser oscillator is therefore sufficient to reach the regime where Newton's equations of motion describe the electron's response quite well; this marks the regime of attosecond science[1]. Field enhancement near nanostructures has also facilitated the generation of high-harmonic radiation from gas atoms with an oscillator only[12], whereas in conventional gas phase experiments amplified laser systems are used[13]. Second, because of the localized nature of field enhancement, electron emission is limited to a single well-defined site with a diameter of $\sim$10 nm, right on the tip's apex. As this is much smaller than the focal diameter of the laser beam, the laser intensity can be well approximated as constant over the electron emission area. Thus electrons are emitted from a single nanometre-sized area exposed to a well-defined laser intensity.

This condition does not usually hold for photoemission from plane surfaces, where local laser intensities differ greatly, owing to the Gaussian profile of the laser beam and hotspot effects due to potential surface roughness. We conjecture that carrier-envelope phase effects are therefore blurred when the electron emission current from a larger area is measured. Presumably for these reasons, only minuscule carrier-envelope phase effects have so far been observed in nonlinear photoemission from a gold cathode, even though extremely short near-infrared laser pulses (with a duration of 4 fs) were used[14]. A previous attempt to measure a carrier-envelope phase dependence in photoemission from sharp tips lacked spectral information, which presumably hindered detection of the signal[15]. An attosecond streaking experiment from a solid has been reported[16], but there the electrons were photoemitted from the metal surface by extreme-ultraviolet pulses before they interacted with the infrared light field, thereby mitigating hotspot effects. Collective electron effects[17] and strong-field effects[18,19] have been observed in tip-enhanced electron emission, while ref. 20 shows that thermal effects can be ruled out here.

In the present experiment, we focus $\sim$6-fs pulses tightly on a tungsten tip; the pulses are derived from a Ti:sapphire oscillator with a stabilized

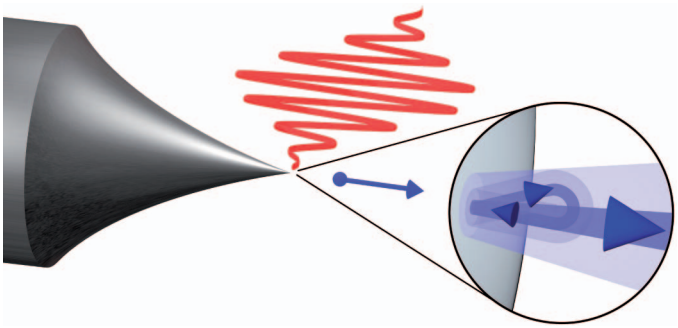

Figure 1 | Overview of the experiment. Electrons, indicated in blue, are emitted (large blue arrow pointing away from surface) from a sharp tungsten tip (left) by, and interact with, a few-cycle laser electric field (red waveform). Controlled by the carrier-envelope phase, the liberated electron may be driven back into the tip, where it can scatter elastically and gain more energy in the laser field before it reaches the detector (not shown).

[1]Ultrafast Quantum Optics Group, Max-Planck-Institut für Quantenoptik, Hans-Kopfermann-Straße 1, D-85748 Garching bei München, Germany.
*These authors contributed equally to this work.

carrier-envelope phase and an 80-MHz repetition rate (Fig. 1; the set-up is described in more detail in ref. 19 and in Supplementary Information). A small negative extraction voltage is applied to the tip, resulting in a d.c. electric field strength of $\sim 0.4\,\mathrm{GV\,m^{-1}}$ at the tip's apex. We record photoelectron spectra with a retarding field spectrometer.

Conclusions can be drawn about the dynamics of the photoelectrons from the overall shape of the spectra. In Fig. 2a, we present a carrier-envelope phase averaged spectrum obtained with 240-pJ pulse energy (a peak intensity of $\sim 4 \times 10^{11}\,\mathrm{W\,cm^{-2}}$ in the bare focus), with an average yield of about one electron per pulse. The spectrum is governed by above-threshold photoemission peaks spaced approximately by the photon energy (1.56 eV) on top of an overall exponential decay[19]. This decay is followed by a plateau, a region of almost constant count rate extending from ~4.5 eV to a soft cut-off located at ~13 eV. The appearance of the plateau indicates that coherent elastic re-scattering of electrons is taking place. This effect is well known in the ionization of atoms in the gas phase: a small fraction of the photoelectrons is driven back into the tip by the laser field, scatters elastically off the tip, and gains more energy in the laser field before being detected[21]. Models presented below strongly support this notion. A more detailed investigation of electron re-scattering dynamics from a metal is currently under way. We note that recombination of the active electron can lead to emission of high-harmonic radiation[1]. We expect this process to also take place at tips.

The electric field of the laser pulses can be written as $E(t) = f(t)\cos(\omega t + \phi_{CE})$, with $f(t)$ describing the pulse envelope, ω the laser's centre (circular) frequency, and ϕ_{CE} the carrier-envelope phase. Figure 2b shows a contour plot of individual electron spectra as a function of the carrier-envelope phase offset, which is given by the sum of ϕ_{CE} and a constant experimental phase difference to be determined by theory (set to 0 here, see below). Clearly, the spectral features are strongly modulated with the carrier-envelope phase: both maxima and minima show pronounced modulation effects with a period of 2π. In Fig. 2a (green points) we display the modulation depth of the count rate for different energy positions (for a definition, see Supplementary Information). At low energy, the modulation depth amounts to several per cent and gains strength in the plateau (10–25%). In the region of the 13-eV cut-off, it increases to ~100% and here the carrier-envelope phase almost completely determines if a photoelectron will be detected.

The visibility of the plateau peaks is particularly strongly affected by the carrier-envelope phase. Figure 2c depicts individual spectra for four carrier-envelope phase settings spaced by $\pi/2$. It is evident that for certain phases peaks are clearly visible, whereas for others the peaks almost completely disappear. An analysis of the average peak visibility is shown in Fig. 2d (for details, see Supplementary Information). It is approximately sinusoidally modulated with the carrier-envelope phase, ranging from ~10% for $\phi_{CE} \approx -0.2\pi$ to ~30% for $\phi_{CE} \approx 0.8\pi$. We will show below that the peaks arise from quantum mechanical interference of electron wave packets re-scattering at the tip in different optical cycles. The visibility can be identified as the degree of spectral interference. Strong interference indicates that (at least) two wave-packet components contribute to the plateau. In contrast, the absence of interference implies that only a single electron wave packet from one optical cycle contributes.

In addition, we observe that the position of the high-energy cut-off changes with carrier-envelope phase, as shown in Fig. 2b (red line). It varies between 12.3 eV and 13.6 eV. Notably, the behaviour of peak visibility and cut-off position is maximally out of phase: the phase difference amounts to $\pi + (80 \pm 160)$ mrad.

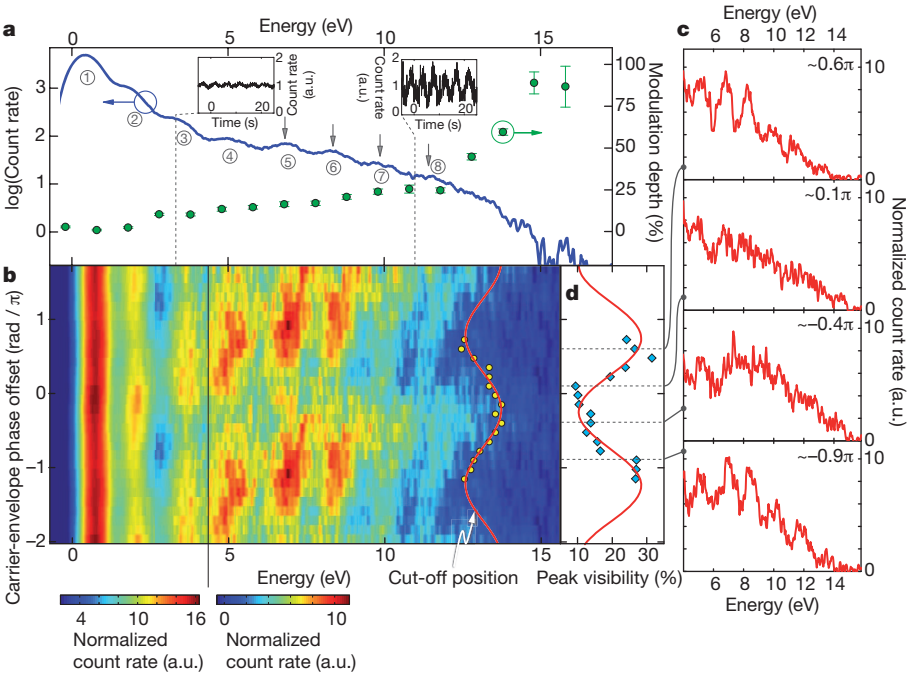

Figure 2 | Carrier-envelope phase modulation in photoelectron spectra. **a**, Carrier-envelope phase-averaged electron count rate as function of energy (blue solid curve). About three photon orders, indicated by encircled numbers, are visible in the direct part (that is, when the electrons do not re-collide with the tip; $E = 0$ to ~4.3 eV). For $E > 4.5$ eV, the plateau region starts with five more photon orders visible. The green points depict the modulation depth of the count rate when varying the carrier-envelope phase (error bars, fit errors of modulation curves; see Supplementary Information). Insets, carrier-envelope phase modulation in the photocurrent with the spectrometer acting as an energy high-pass filter at 3 eV (left inset) and 11 eV (right inset; both with the carrier-envelope offset frequency set to $f_{CEO} = \dot{\phi}_{CE}/2\pi = 0.2$ Hz). a.u., arbitrary units. **b**, Contour plot of the electron count rate as function of carrier-envelope phase offset and energy. ϕ_{CE} was increased in steps of $\pi/8$. At 4.3 eV, the plot is split into two regions for better visibility (see colour scales under). In each region, we plot the normalized count rate (Supplementary Information). Measured data range over 2π and are extended over $\sim 4\pi$ for better visibility. Yellow circles show the position of the cut-off for a given carrier-envelope phase offset (red curve, sinusoidal fit). **c**, Individual electron spectra extracted from the contour plot in **b** for four different carrier-envelope phase offsets separated by $\pi/2$. Only the plateau region is shown. Fringes are clearly visible for 0.6π and -0.9π, but almost no fringes are visible for 0.1π and -0.4π. **d**, Blue diamonds, average peak visibility in the plateau region (red curve, sinusoidal fit). The peaks used to determine the visibility are marked with grey arrows in **a**. Note that peak visibility and cut-off position are nearly maximally out of phase.

We interpret our experimental findings with the aid of two theoretical models. The first model used is the semiclassical Simple Man's Model (SMM)[22]. In brief, an electron is liberated by optically induced tunnelling and subsequently propagates in the laser electric field on classical trajectories. The model has been extended to account for the matter-wave nature of liberated electrons by including the accumulated quantum mechanical phase of the corresponding wave packets[23]. Trajectories with different start times within the pulse that lead to the same final energy interfere, resulting in interference structures in the energy domain[24].

In Fig. 3a we present spectra simulated by the SMM that are similar to those in Fig. 2b; we assume a 6.3-fs pulse with a peak electric field of 10.4 GV m^{-1}. All the main features of the experimental data are qualitatively reproduced, notably the shift of the cut-off position and the correlated change in peak visibility. A region is observed where no spectral interference occurs, centred around $\phi_{CE} \approx 0$, corresponding to a 'cosine-like' pulse. Simultaneously, the cut-off position is located at the highest energy. Figure 3b illustrates the physical origin of both effects (namely, no spectral interference and the cut-off position located at the highest energy) for $\phi_{CE} \approx 0$: only a single trajectory from one optical half-cycle, reaching the highest possible kinetic energy, yields a significant contribution to the electron count rate in the high-energy part of the spectrum. In contrast, the region around $\phi_{CE} \approx \pm\pi$, which corresponds to a 'minus-cosine-like' pulse, exhibits the strongest peak structure and the lowest cut-off energy. Two trajectories from subsequent cycles contribute here, with the times of both emission and re-scattering differing approximately by the duration of an optical cycle, T_{opt}. This translates into interference fringes in the energy domain, with a spacing of $\Delta E \approx h/T_{opt} = h/(2.67\ \text{fs}) \approx 1.56$ eV, approximately equalling the photon energy[23]. A similar behaviour was demonstrated for strong-field photoemission from atomic gases[24], and also in ref. 25, where the generation of single subfemtosecond extreme-ultraviolet radiation bursts was deduced from the absence of interference in the cut-off region of the extreme-ultraviolet spectrum. Accordingly, single electron matter-wave packets with initially subfemtosecond emission duration (Fourier limit of cut-off part, ~450 as) can be generated from a metallic tip by appropriate setting of the carrier-envelope phase. Moreover, the timing of the emission and propagation of electron wave packets undergoing re-scattering near the metal surface can be controlled with a precision of ~80 as by changing the carrier-envelope phase, as inferred from the error of the phase offset in the sinusoidal fits to cut-off and visibility. The presence of interference indicates the coherent nature of the re-scattering process off a metal surface, which has not been reported before.

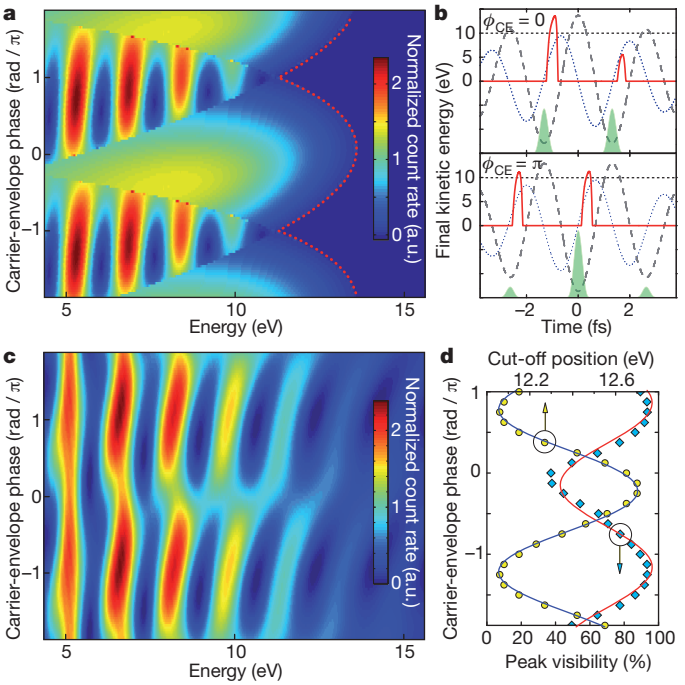

Figure 3 | Theoretical modelling of the experimental data. **a**, Contour plot representation of the count rate as a function of energy and carrier-envelope phase, according to the extended SMM. Here only re-scattered electrons are considered (only those contribute to plateau energies). Regions with quantum mechanical interference fringes ($\phi_{CE} \approx \pm\pi$) and without ($\phi_{CE} \approx 0$) are evident (sharp borders reflect the semiclassical nature of the model). Furthermore, the highest electron energies are reached for carrier-envelope phase settings corresponding approximately to the most featureless electron spectrum ($\phi_{CE} \approx 0$). Dotted red curve, the classical cut-off position. **b**, Final kinetic energy (red curve) and emission probability (green area) as a function of emission time for phases 0 and π. The emission probability in the model follows the electric field (dashed grey curve). Emission occurs only when the electric field is negative and points into the metal, thus pulling electrons out of the metal. The electron's kinematics can be inferred more easily from the light field's vector potential $A(t)$, shown with a blue dotted line ($E(t) = -\partial A(t)/\partial t$). Notably, either one or two trajectories contribute significantly to the kinetic energy of, for example, 10 eV (marked by the dotted horizontal lines). Within each cycle a second trajectory also exists, but the corresponding emission probability can be neglected with respect to the dominating one. **c**, As in **a** but calculated by numerically integrating the TDSE. **d**, Average peak visibility and cut-off position from **c**.

The second model, a fully quantum mechanical treatment, shows good quantitative agreement with the experiment. In Fig. 3c we present energy spectra retrieved from a numerical integration of the one-dimensional time-dependent Schrödinger equation (TDSE)[15]. The parameters were adapted to match the experimental data (see Supplementary Information for details). The average peak visibility and the cut-off position are depicted in Fig. 3d and behave similarly to the experimental data. We have shifted the carrier-envelope phase axis of the experimental data so that the maxima of the cut-off position curves coincide, thereby zeroing the experimental phase offset. Thus, the pulse is cosine-like ($\phi_{CE} = 0$) for a carrier-envelope phase offset of $(0.00 \pm 0.05)\pi$. The spectral shift of the cut-off with carrier-envelope phase in the TDSE model is a weaker effect (peak-to-peak shift ~0.7 eV) than in the experimental data (peak-to-peak shift ~1.3 eV, compare Fig. 3d and Fig. 2b), mainly because strong smoothing had to be applied to the TDSE spectra in order to suppress effects caused by the pronounced peak structure. The SMM (Fig. 3a), in contrast, reveals a larger shift (peak-to-peak ~2.3 eV), mainly due to its semiclassical nature. Given the simplicity of the models, the agreement is satisfactory.

The peak visibility is lower in the experiment than in both theoretical treatments, which we attribute to the spectrometer resolution and low counting statistics. Moreover, in both models we consider only a single initial electronic state at the Fermi level. A metal, however, comprises many populated states with a large spread of initial energies. In future work, a more elaborate simulation[7,8] will be needed to fully take this into account, together with possible plasmonic effects; the technique could then be used to draw conclusions about the underlying subfemtosecond dynamics.

Three points are noteworthy. First, the observable carrier-envelope phase of the enhanced field at the tip's surface should be phase-shifted with respect to the phase of the driving laser field, owing to the plasmonic response of the metal[8,12]. Spectra measured from a tip with strong plasmonic behaviour (such as one made from silver) would thus allow information to be obtained about the collective electron response on the subnanometre–subfemtosecond scale. Second, in the SMM, an emission process according to optically induced tunnelling has been assumed, with the electrons' classical trajectories starting at the tunnel exit with zero initial momentum[6,26] and with an emission probability modelled along the lines of the ADK rate (see Supplementary Information). We also tried other emission processes (non-adiabatic tunnelling[27], multiphoton photoemission) but found the best agreement using tunnelling, although here the Keldysh parameter is

~2. We stress that in this parameter range, the emission process encompasses and cannot be separated from strong-field effects after the electron has been classically emitted. Third, although the exact quantum dynamics of electrons in this new system is complex and to understand it fully will require much further investigation, it has become clear from experiments with neutral atoms[21] and negatively charged ions[28] that the re-scattering scheme and the concomitant telltale plateau seem to be universal, in the sense that they exist despite qualitatively different potentials (long[21] versus short range[28]). Also, we note that related initial theoretical work on photoemission from metals contains hints in this direction[29]. Our experimental results provide strong evidence for very similar underlying physics, even though here the dimensions involved are very different from those involved in studies on atoms or ions: the electron source and scatterer, namely the solid tip, is much larger than the classical oscillation amplitude of the electron in the laser field (a few ångströms). It will be interesting to investigate the implications of this. For example, does scattering take place at the extended surface or at individual surface atoms—and does this depend on the material and its orientation? Angle-resolved spectra might yield information.

With longer laser wavelengths, the energy of the re-colliding electron increases and can surpass several tens of electron volts. Hence, new forms of (time-resolved) surface science techniques—such as low-energy electron diffraction—with electrons originating from and probing the surface, might come into reach, with typical timescales of 100 as. Extending this work towards more complex, lithographically grown nanoscale objects[11,30] will pave the way to lightwave electronics, where the electric field of light steers electrons; for example, the area between a source and a drain electrode could be switched between conducting and insulating states. Also, a simple stand-alone die-sized (1-cm^3) sensor device for the carrier-envelope phase might be feasible: such a device could be extremely sensitive, and comprise only a tip, a retardation grid and an electron multiplier.

Received 22 February; accepted 12 May 2011.

1. Corkum, P. B. & Krausz, F. Attosecond science. *Nature Phys.* **3,** 381–387 (2007).
2. Antoine, P., L'Huillier, A. & Lewenstein, M. Attosecond pulse trains using high-order harmonics. *Phys. Rev. Lett.* **77,** 1234–1237 (1996).
3. Goulielmakis, E. *et al.* Single-cycle nonlinear optics. *Science* **320,** 1614–1617 (2008).
4. Niikura, H. *et al.* Sub-laser-cycle electron pulses for probing molecular dynamics. *Nature* **417,** 917–922 (2002).
5. Baker, S. *et al.* Probing proton dynamics in molecules on an attosecond time scale. *Science* **312,** 424–427 (2006).
6. Huismans, Y. *et al.* Time-resolved holography with photoelectrons. *Science* **331,** 61–64 (2011).
7. Lemell, C., Tong, X.-M., Krausz, F. & Burgdörfer, J. Electron emission from metal surfaces by ultrashort pulses: determination of the carrier-envelope phase. *Phys. Rev. Lett.* **90,** 076403 (2003).
8. Stockman, M. I. & Hewageegana, P. Absolute phase effect in ultrafast optical responses of metal nanostructures. *Appl. Phys. A* **89,** 247–250 (2007).
9. Stockman, M. I. Nanofocusing of optical energy in tapered plasmonic waveguides. *Phys. Rev. Lett.* **93,** 137404 (2004).
10. Goulielmakis, E. *et al.* Attosecond control and measurement: lightwave electronics. *Science* **317,** 769–775 (2007).
11. Novotny, L. & van Hulst, N. Antennas for light. *Nature Photon.* **5,** 83–90 (2011).
12. Kim, S. *et al.* High-harmonic generation by resonant plasmon field enhancement. *Nature* **453,** 757–760 (2008).
13. Bucksbaum, P. H. The future of attosecond spectroscopy. *Science* **317,** 766–769 (2007).
14. Apolonski, A. *et al.* Observation of light-phase-sensitive photoemission from a metal. *Phys. Rev. Lett.* **92,** 073902 (2004).
15. Hommelhoff, P., Kealhofer, C. & Kasevich, M. A. Ultrafast electron pulses from a tungsten tip triggered by low-power femtosecond laser pulses. *Phys. Rev. Lett.* **97,** 247402 (2006).
16. Cavalieri, A. L. *et al.* Attosecond spectroscopy in condensed matter. *Nature* **449,** 1029–1032 (2007).
17. Yanagisawa, H. *et al.* Optical control of field-emission sites by femtosecond laser pulses. *Phys. Rev. Lett.* **103,** 257603 (2009).
18. Bormann, R., Gulde, M., Weismann, A., Yalunin, S. V. & Ropers, C. Tip-enhanced strong-field photoemission. *Phys. Rev. Lett.* **105,** 147601 (2010).
19. Schenk, M., Krüger, M. & Hommelhoff, P. Strong-field above-threshold photoemission from sharp metal tips. *Phys. Rev. Lett.* **105,** 257601 (2010).
20. Kealhofer, C., Foreman, S. M., Gerlich, S. & Kasevich, M. A. Ultrafast laser-triggered emission from hafnium carbide tips. *Phys. Rev. B* (submitted); preprint at ⟨http://arxiv.org/abs/1104.1452⟩ (2011).
21. Paulus, G. G., Nicklich, W., Xu, H. L., Lambropoulos, P. & Walther, H. Plateau in above-threshold ionization spectra. *Phys. Rev. Lett.* **72,** 2851–2854 (1994).
22. Corkum, P. B. Plasma perspective on strong-field multiphoton ionization. *Phys. Rev. Lett.* **71,** 1994–1997 (1993).
23. Milošević, D. B., Paulus, G. G., Bauer, D. & Becker, W. Above-threshold ionization by few-cycle pulses. *J. Phys. B* **39,** R203–R262 (2006).
24. Lindner, F. *et al.* Attosecond double-slit experiment. *Phys. Rev. Lett.* **95,** 040401 (2005).
25. Baltuška, A. *et al.* Attosecond control of electronic processes by intense light fields. *Nature* **421,** 611–615 (2003).
26. Zherebtsov, S. *et al.* Controlled near-field enhanced electron acceleration from dielectric nanospheres with intense few-cycle laser fields. *Nature Phys.* advance online publication, doi:10.1038/nphys1983 (24 April 2011).
27. Yudin, G. L. & Ivanov, M. Y. Nonadiabatic tunnel ionization: looking inside a laser cycle. *Phys. Rev. A* **64,** 013409 (2001).
28. Gazibegović-Busuladžić, A. *et al.* Electron rescattering in above-threshold photodetachment of negative ions. *Phys. Rev. Lett.* **104,** 103004 (2010).
29. Faisal, F. H. M., Kamiński, J. Z. & Saczuk, E. Photoemission and high-order harmonic generation from solid surfaces in intense laser fields. *Phys. Rev. A* **72,** 023412 (2005).
30. Aeschlimann, M. *et al.* Adaptive subwavelength control of nano-optical fields. *Nature* **446,** 301–304 (2007).

Supplementary Information is linked to the online version of the paper at www.nature.com/nature.

Acknowledgements We thank M. Kling, C. Lemell, G. Wachter and B. Bergues for discussions, and J. Hoffrogge for reading the text before submission. This work has been supported in part by the European Union (FP7-IRG).

Author Contributions All authors contributed to all parts of the work.

Author Information Reprints and permissions information is available at www.nature.com/reprints. The authors declare no competing financial interests. Readers are welcome to comment on the online version of this article at www.nature.com/nature. Correspondence and requests for materials should be addressed to P.H. (peter.hommelhoff@mpq.mpg.de).